Optics Letters

# Realization of maximum optical intrinsic chirality with bilayer polyatomic metasurfaces

Xi Zhao,[1] Zhancheng Li,[1,4] Jiaqi Cheng,[1] Wenwei Liu,[1] Shiwang Yu,[1] Yuebian Zhang,[1] Hua Cheng,[1,5] Jianguo Tian,[1,6] and Shuqi Chen[1,2,3,*]

[1]The Key Laboratory of Weak Light Nonlinear Photonics, Ministry of Education, Renewable Energy Conversion and Storage Center, School of Physics and TEDA Institute of Applied Physics, Nankai University, Tianjin 300071, China
[2]The Collaborative Innovation Center of Extreme Optics, Shanxi University, Taiyuan, Shanxi 030006, China
[3]Collaborative Innovation Center of Light Manipulations and Applications, Shandong Normal University, Jinan 250358, China
[4]e-mail: zcli@nankai.edu.cn
[5]e-mail: hcheng@nankai.edu.cn
[6]e-mail: jjtian@nankai.edu.cn
*Corresponding author: schen@nankai.edu.cn

Received 4 July 2022; revised 3 August 2022; accepted 23 August 2022; posted 23 August 2022; published 14 September 2022

**Optical chirality plays a key role in optical biosensing and spin-selective optical field manipulation. However, the maximum optical intrinsic chirality, which is represented by near-unity circular dichroism (CD), is yet to be achieved in a wide bandwidth range based on nanostructures. Here, we utilize dielectric bilayer polyatomic metasurfaces to realize the maximum optical intrinsic chirality over a wide bandwidth range. The CD efficiency of the two designed metasurfaces with opposite chirality is 99.9% at 1350 nm and over 98% from 1340 nm to 1361 nm. Our work provides a straightforward and powerful method for the realization of maximum optical intrinsic chirality, which has great potential in spin-selective optical wave manipulation.** 

https://doi.org/10.1364/OL.469518

Chirality refers to a geometric property of objects that cannot coincide with their mirror counterparts. Chiral materials interact differently with left-handed and right-handed circularly polarized (LCP and RCP) waves, resulting in chiral optical responses such as optical activity and circular dichroism (CD). The CD characterized by different scattering properties of chiral materials under LCP and RCP illuminations serves as the main method for the detection and discrimination of chirality. However, the CD of natural materials is quite subtle due to the mismatch in size between molecules and the wavelength of optical waves. Recently, metasurfaces composed of artificial nanostructures at the subwavelength scale have emerged as a powerful platform for the enhancement of CD, because the size of nanostructures is comparable to the wavelength of optical waves and their structural symmetry can be arbitrarily designed [1–4]. Metasurfaces composed of three-dimensional or few-layer metallic nanostructures have been demonstrated as good alternatives for the realization of giant CD, which show unprecedented application possibilities in chiral sensing and spin-selective optical wave manipulation [5–16]. Although CD can be greatly enhanced in metasurfaces composed of metallic nanostructures, their intrinsic loss prevents the implementation of near-unity CD ($T_{\mathrm{RCP}} - T_{\mathrm{LCP}} \approx \pm 1$).

Near-unity CD, representing the maximum optical intrinsic chirality, describes the objects which are transparent to normally incident optical waves with one helicity while completely scattering the normally incident optical waves with the other helicity [17,18]. Recent advances in dielectric metasurfaces proved that they can overcome the lossy defect of metallic metasurfaces and realize near-unity CD [19–22]. Giant CD with near 90% efficiency was realized at 540 nm by utilizing a dielectric metasurface composed of gammadion nanostructures, which is almost transparent to normally incident RCP waves while diffracting the LCP waves into the first order [19]. Meanwhile, CD with over 70% efficiency was demonstrated in the near-infrared band based on a bilayer dielectric metasurface [20]. Recently, near-unity CD was realized in dielectric metasurfaces based on chiral bound states in the continuum [21,22]. However, the bandwidth, corresponding to CD with over 90% efficiency, is narrower than 1.5 nm by this approach. The CD efficiency is extremely sensitive to some structural parameters and the absorption loss of the dielectric materials. The realization of near-unity CD in a wide bandwidth range still remains a challenge.

Here, we demonstrate the use of bilayer polyatomic metasurfaces for the realization of near-unity CD in a wide bandwidth range. The near-unity CD of the proposed metasurfaces is achieved by exploiting the spin-selective destructive and constructive interferences of optical waves in polyatomic metasurfaces, which can be treated as a result of the combination of two near-perfect circular polarization conversion processes. We also validate that the layer effects in the designed metasurfaces can improve the efficiency of CD.

The Jones transmission matrix (in the $-z$ direction) of an object with CD = 1 can be expressed as

$$\mathbf{T}_{\mathrm{circ}}^{\mathrm{MLC}} = \begin{bmatrix} T_{\mathrm{LL}} & T_{\mathrm{LR}} \\ T_{\mathrm{RL}} & T_{\mathrm{RR}} \end{bmatrix} = \begin{bmatrix} 0 & 0 \\ 0 & 1 \end{bmatrix}, \quad (1)$$

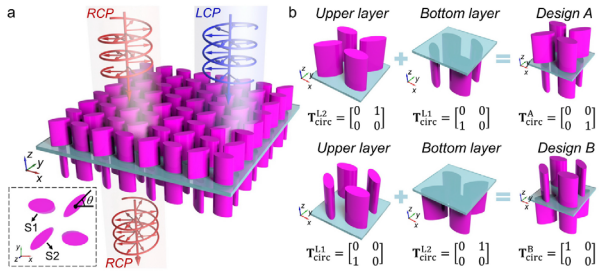


**Fig. 1.** Design strategy of bilayer polyatomic metasurfaces with maximum optical intrinsic chirality. (a) Schematic of a designed metasurface with CD = 1, which is transparent to RCP waves and reflects all of the LCP waves. Inset: top view of one unit cell on the upper layer. (b) Illustration of the design strategy.

where the subscript "circ" indicates that the transmission matrix lies in the circular base, while the superscript "MLC" represents the maximum left-handed optical intrinsic chirality. The subscripts "$i$" and "$j$" of $T_{ij}$ indicate the circularly polarization states of the transmission and incident waves, respectively. The matrix in Eq. (1) can be further decomposed into two symmetric matrices:

$$\mathbf{T}_{\mathrm{circ}}^{\mathrm{MLC}} = \mathbf{T}_{\mathrm{circ}}^{1}\mathbf{T}_{\mathrm{circ}}^{2} = \begin{bmatrix} 0 & 0 \\ 1 & 0 \end{bmatrix} \cdot \begin{bmatrix} 0 & 1 \\ 0 & 0 \end{bmatrix}. \tag{2}$$

For bilayer metasurfaces composed of layered nanostructures with negligible reflectance, the multiwave interference effect between the layers can be ignored. The transmission matrices of such bilayer metasurfaces can be mathematically calculated as the product of the transmission matrix of each layer. Here, the phase delay caused by the spacer between the layers is neglected. If we can find two single-layer metasurfaces whose transmission matrices equal $\mathbf{T}_{\mathrm{circ}}^{1}$ and $\mathbf{T}_{\mathrm{circ}}^{2}$, the transmission matrix of the bilayer metasurface composed of these two single-layer nanostructures can be the same as the one in Eq. (1). The single-layer nanostructures with transmission matrices of $\mathbf{T}_{\mathrm{circ}}^{1}$ and $\mathbf{T}_{\mathrm{circ}}^{2}$ can be treated as perfect LCP to RCP and RCP to LCP polarization converters, respectively. Such a circular polarization converter can be well implemented by using polyatomic metasurfaces. The polyatomic metasurfaces are planar arrays whose unit cell is composed of multiple functional nanostructures [23–25]. They can significantly expand the design freedom of metasurfaces and be demonstrated as an appealing alternative for multidimensional optical wave manipulation.

Figure 1 is an illustration of the designed bilayer polyatomic metasurfaces. The designed metasurfaces are transparent to normally incident waves with one helicity while completely scattering normally incident optical waves with the other helicity. Figure 1(a) is a schematic of the designed metasurface with CD = 1, which is composed of two kinds of single-layer polyatomic nanostructures (L1 and L2) on a $SiO_2$ substrate. Each polyatomic nanostructure consists of two kinds of $\alpha$-Si elliptical nanocylinders (S1 and S2) with different structural parameters, and the relative rotation angle $\theta$ between them equals $-45°$ and $45°$ for L1 and L2, respectively. We assume that the optical wave propagates along the $-z$ direction. The two elliptical nanocylinders with long axes along the $x$ direction are firstly designed as two perfect half-wave plates with $\pi/2$ phase delay, which can be described by the Jones transmission matrices [26]:

$$\mathbf{T}_{\mathrm{circ}}^{\mathrm{S1}} = \mathrm{e}^{-i\frac{\pi}{2}} \cdot \begin{bmatrix} 0 & 1 \\ 1 & 0 \end{bmatrix}, \tag{3a}$$

$$\mathbf{T}_{\mathrm{circ}}^{\mathrm{S2}} = \begin{bmatrix} 0 & 1 \\ 1 & 0 \end{bmatrix}. \tag{3b}$$

The transmission matrix of S2 with a rotation angle $\theta$ of $-45°$ or $45°$ along the $z$ axis then can be expressed as

$$\mathbf{T}_{\mathrm{circ}}^{\mathrm{S2}(-45°)} = \mathrm{e}^{-i\frac{\pi}{2}} \cdot \begin{bmatrix} 0 & -1 \\ 1 & 0 \end{bmatrix}, \tag{4a}$$

$$\mathbf{T}_{\mathrm{circ}}^{\mathrm{S2}(45°)} = \mathrm{e}^{-i\frac{\pi}{2}} \cdot \begin{bmatrix} 0 & 1 \\ -1 & 0 \end{bmatrix}. \tag{4b}$$

The transmission matrices of the two polyatomic nanostructures L1 and L2 composed of these two elliptical nanocylinders can be derived as

$$\mathbf{T}_{\mathrm{circ}}^{\mathrm{L1}} = \frac{1}{2}(\mathbf{T}_{\mathrm{circ}}^{\mathrm{S1}} + \mathbf{T}_{\mathrm{circ}}^{\mathrm{S2}(-45°)}) = \mathrm{e}^{-i\frac{\pi}{2}} \cdot \begin{bmatrix} 0 & 0 \\ 1 & 0 \end{bmatrix}, \tag{5a}$$

$$\mathbf{T}_{\mathrm{circ}}^{\mathrm{L2}} = \frac{1}{2}(\mathbf{T}_{\mathrm{circ}}^{\mathrm{S1}} + \mathbf{T}_{\mathrm{circ}}^{\mathrm{S2}(45°)}) = \mathrm{e}^{-i\frac{\pi}{2}} \cdot \begin{bmatrix} 0 & 1 \\ 0 & 0 \end{bmatrix}. \tag{5b}$$

In the polyatomic nanostructure L1, the converted LCP waves from S1 and S2 under RCP illumination have a phase difference of $\pi$. They destructively interfere with each other, resulting in the elimination of transmittance. The converted RCP waves from S1 and S2 under LCP illumination have no phase difference. They constructively interfere with each other, resulting in high transmittance. The situation is opposite for the polyatomic nanostructure L2. Therefore, the two polyatomic nanostructures are perfect LCP to RCP and RCP to LCP converters. As shown in Fig. 1(b), by arranging the two polyatomic nanostructures in two layers, the transmission matrices of the designed bilayer polyatomic metasurfaces (designs A and B) can be expressed as

$$\mathbf{T}_{\mathrm{circ}}^{\mathrm{A}} = \mathbf{T}_{\mathrm{circ}}^{\mathrm{L1}} \cdot \mathbf{T}_{\mathrm{circ}}^{\mathrm{L2}} = \mathrm{e}^{-i\pi} \cdot \begin{bmatrix} 0 & 0 \\ 0 & 1 \end{bmatrix}, \tag{6a}$$

$$\mathbf{T}_{\mathrm{circ}}^{\mathrm{B}} = \mathbf{T}_{\mathrm{circ}}^{\mathrm{L2}} \cdot \mathbf{T}_{\mathrm{circ}}^{\mathrm{L1}} = \mathrm{e}^{-i\pi} \cdot \begin{bmatrix} 1 & 0 \\ 0 & 0 \end{bmatrix}. \tag{6b}$$

Therefore, designs A and B can realize maximum left-handed and right-handed intrinsic optical chirality (CD = 1 and −1), respectively. According to Eq. (6), the realization of |CD| = 1 in the designed metasurfaces can be regarded as a result of the combination of two perfect circular polarization conversion processes. Taking design A as an example, when LCP and RCP waves illuminate from the $-z$ direction, the upper layer will reflect the LCP waves, and the RCP waves will be fully converted into LCP transmitted waves. Then, the converted LCP waves will be further fully converted into RCP waves by the lower layer. Overall, design A is transparent to normally incident RCP waves while completely scattering normally incident LCP waves. Note that the optical responses of designs A and B do not change when the waves illuminate along the $+z$ direction. When the optical waves illuminate from the $+z$ direction, the relative rotation angle $\theta$ between the elliptical nanocylinders in the bottom layer will change from $-45°$ to $45°$, while that in the upper layer will change from $45°$ to $-45°$. As a result, the transmission matrix of design A in the $+z$ direction is the same as that in the $-z$ direction, resulting in the absence of circular conversion dichroism.

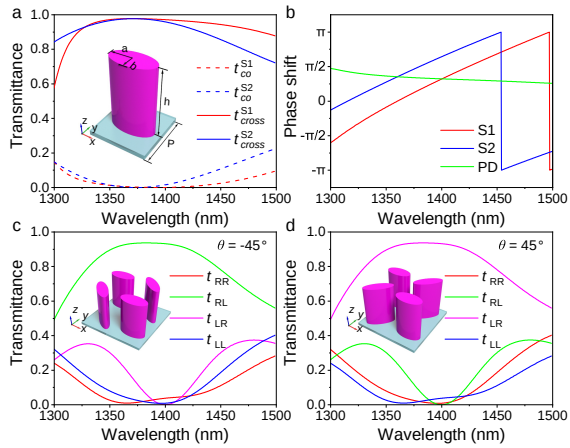


**Fig. 2.** Collective interference-induced circular conversion dichroism in single-layer polyatomic metasurfaces. Optical response of the two kinds of elliptical nanocylinders S1 and S2 as the component of polyatomic metasurfaces: (a) simulated results of the cross- and co-components of the circularly polarized transmission spectra and (b) simulated phase shifts of the cross-polarized transmission waves and the calculated phase difference (PD), under circularly polarized illuminations along the $-z$ direction. Simulated transmission spectra of the two designed single-layer polyatomic metasurfaces with (c) $\theta = -45°$ and (d) $\theta = 45°$ under illuminations along the $-z$ direction for different incident/output helicity combinations.

The simulated optical responses of the designed elliptical nanocylinders and single-layer polyatomic nanostructures are presented in Fig. 2. As shown in the inset of Fig. 2(a), the structural parameters of the two designed elliptical nanocylinders S1 and S2 are: $a_1 = 230$ nm, $a_2 = 230$ nm, $b_1 = 107.5$ nm, $b_2 = 80$ nm, $h = 710$ nm, and $P = 565$ nm, where $a_1$ ($a_2$) and $b_1$ ($b_2$) are half the lengths of the long and short axes of elliptical nanocylinder S1 (S2). The polyatomic nanostructures L1 and L2 [as shown in the insets of Figs. 2(c) and 2(d)] are composed of the two elliptical nanocylinders, in which the long axis of S1 is along the $x$ axis and the long axis of S2 has a relative rotation angle $\theta$ of $-45°$ (in L1) or $45°$ (in L2). The simulated results were obtained using a full-wave simulation based on the finite element method. The refractive index of $SiO_2$ was set to be 1.5 and the refractive index of $\alpha$-Si was obtained from experimentally measured data [27]. Since the near-field interaction between the dielectric elliptic nanocylinders is weak, the transmission matrices of periodic arrays are used to approximate the transmission matrices of isolated nanostructures [24,26]. The results in Fig. 2(a) validate that the two designed elliptical nanocylinders can be treated as high-efficiency half-wave plates, for which the transmittances of cross-polarized waves are much larger than those of co-polarized waves under circularly polarized illuminations. The phase difference between the cross-polarized waves from S1 and S2 is wavelength-dependent and changes from $\pi/2$ to $\pi/4$ with an increase of wavelength, as shown in Fig. 2(b). The phase delay between S1 and S2 is not equal to $\pi/2$ since the structural parameters of the two designed elliptical nanocylinders were secondarily optimized to offset the influence of near-neighbor interaction between the elliptical nanocylinders in the designed single-layer polyatomic nanostructures on the transmission coefficients. The squared moduli $t_{ij} = |T_{ij}|^2$ of the coefficients in the transmission matrices (in the $-z$ direction) of the two designed polyatomic nanostructures L1 and L2 are presented in Figs. 2(c) and 2(d), respectively. For polyatomic nanostructure L1 with $\theta = -45°$, $t_{RL}$ is over 0.9 at 1400 nm while $t_{RR} = 0.01$, $t_{LR} = 10^{-5}$, and $t_{LL} = 0.04$. Therefore, L1 can be regarded as a near-perfect LCP to RCP polarization converter around 1400 nm. Similarly, L2 can be treated as a near-perfect RCP to LCP polarization converter around 1400 nm.

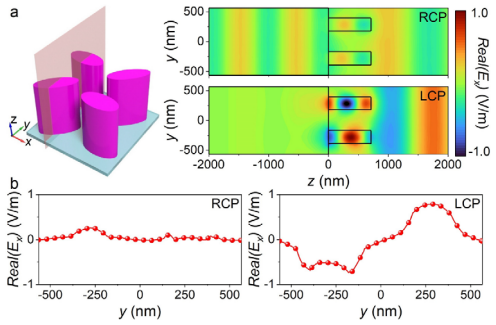


**Fig. 3.** Collective interference of optical waves in polyatomic nanostructure L2. (a) Cross-sectional distributions of the electric field $E_x$ under the illumination of RCP (top right) and LCP (bottom right) waves from the $-z$ direction at a wavelength of 1400 nm. (b) Distribution of the electric field $E_x$ in (a) along the $y$ axis ($z = -10$ nm) under RCP (left) and LCP (right) illuminations.

To make a further visual demonstration of the constructive and destructive interferences of optical waves between different elliptical nanocylinders, we calculated the cross-sectional distribution of the real part of the $x$ component of electric field $E_x$ at the $y$–$z$ plane ($x = -282.5$ nm) for RCP and LCP waves along the $-z$ direction at 1400 nm, as shown in Fig. 3(a). Results validate that the transmission waves from the two kinds of elliptical nanocylinders under RCP illumination are in phase, leading to the constructive interference of optical waves; on the contrary, the transmission waves from the two kinds of elliptical nanocylinders under LCP illumination are out of phase, leading to the destructive interference of optical waves. We also present the distribution of the real part of $E_x$ along the $y$ axis ($z = -10$ nm, $x = -282.5$ nm) in Fig. 3(b). The quantitative results further support the above statements.

Two designed polyatomic nanostructures can be used to construct bilayer polyatomic metasurfaces with maximum optical intrinsic chirality. The structural configurations of the two designed metasurfaces (designs A and B) are shown in the insets of Figs. 4(a) and 4(b). The thickness $d$ of the $SiO_2$ spacer is 50 nm. Figures 4(a) and 4(b) show the squared moduli of the coefficients in the transmission matrices of the two designed metasurfaces. Since $t_{RR}$ of design A and $t_{LL}$ of design B are close to 1 and the other squared moduli of transmission coefficients are near zero around 1350 nm, they show left-handed and right-handed maximum optical intrinsic chirality, respectively. We calculated the CD $= t_{RCP} - t_{LCP} = (t_{RR} + t_{LR}) - (t_{LL} + t_{RL})$ for designs A and B, as shown in Fig. 4(c). Circular conversion dichroism is nonexistent in both designs A and B at the wave band of interest because $t_{LR}$ and $t_{RL}$ are equal to each other. Designs A and B show left-handed and right-handed chirality, respectively, with CD efficiency of 99.9% at 1350 nm and over 98% from 1340 nm to 1361 nm. Compared with representative works on CD enhancement in metasurfaces based on the resonant multipolar modulation [7,19,20], the plasmonic resonance

[16], or the chiral bound state in the continuum [21], the bilayer polyatomic metasurfaces designed based on our strategy have great advantages in both efficiency and operational bandwidth.

The transmission matrices of designs A and B can be mathematically calculated as the product of the transmission matrix of each layer. Therefore, $t_{RR}$ of design A and $t_{LL}$ of design B should be no more than 0.85 since $t_{RL}$ of L1 and $t_{LR}$ of L2 are less than 0.92. We attribute the increase of $t_{RR}$ of design A and $t_{LL}$ of design B to the existence of near-field interaction and multiwave interference effect between the bilayers since all $t_{ij}$ are not equal to zero and the thickness of the $SiO_2$ spacer is thin. To make a validation, we investigate the variation of CD of design A with changing of wavelength and thickness $d$ of $SiO_2$, as shown in Fig. 4(d). The value of CD slightly decreases with an increase of $d$ around a wavelength of 1350 nm, proving the existence of the near-field interaction between the layers. Meanwhile, the CD spectra change periodically with the variation of $d$, which relates to the multiwave interference effect between the layers [28]. Resonances related to the multiwave interference effect appear with the change of $d$, resulting in the decrease of CD at some narrow wave bands. These narrow wave bands are red-shifted with the increase of $d$, which is a typical characteristic of the multiwave interference effect in few-layer metasurfaces. The layer effects enhance the optical intrinsic chirality of the designed metasurfaces.

In conclusion, we theoretically proposed and numerically demonstrated a new metasurface design strategy based on the wave collective interference effect for the implementation of near-unity CD. The two designed bilayer polyatomic metasurfaces can realize maximum left-handed and right-handed optical intrinsic chirality across a wide bandwidth range in the near-infrared regime, with CD efficiency of 99.9% at 1350 nm and over 98% from 1340 nm to 1361 nm. We also validated that the layer effects in the designed metasurfaces enhance the CD efficiency. The design strategy we proposed here can be further used for the design of chiral metasurfaces in other bands.

**Funding.** National Key Research and Development Program of China (2021YFA1400601); National Science Fund for Distinguished Young Scholars (11925403); National Natural Science Foundation of China (11904181, 11904183, 11974193, 12104243, 12122406, 12192253); Natural Science Foundation of Tianjin City for Distinguished Young Scientists (18JCJQJC45700); China Postdoctoral Science Foundation (2018M640224, 2021M690084).

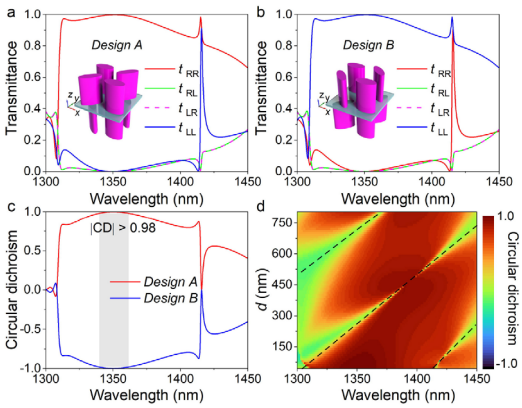


**Fig. 4.** Maximum optical intrinsic chirality of the designed bilayer polyatomic metasurfaces. Simulated transmission spectra of (a) design A and (b) design B. (c) Calculated CD of designs A and B. The gray area represents wavelengths with |CD| larger than 0.98. (d) Variation of CD as a function of the thickness $d$ of the dielectric spacer and wavelength. The black dashed lines represent the resonant wavelengths related to multiwave interference effect at different $d$.

**Disclosures.** The authors declare no conflicts of interest.

**Data availability.** Data underlying the results presented in this paper are not publicly available at this time but may be obtained from the authors upon reasonable request.

## REFERENCES

1. Y. Chen, W. Du, Q. Zhang, O. Ávalos-Ovando, J. Wu, Q. H. Xu, N. Liu, H. Okamoto, A. O. Govorov, Q. Xiong, and C. W. Qiu, Nat. Rev. Phys. **4**, 113 (2022).
2. M. Qiu, L. Zhang, Z. Tang, W. Jin, C. W. Qiu, and D. Y. Lei, Adv. Funct. Mater. **28**, 1803147 (2018).
3. Y. Luo, C. Chi, M. Jiang, R. Li, S. Zu, Y. Li, and Z. Fang, Adv. Opt. Mater. **5**, 1700040 (2017).
4. X. Wang, Small **13**, 1601115 (2017).
5. J. K. Gansel, M. Thiel, M. S. Rill, M. Decker, K. Bade, V. Saile, G. Freymann, S. Linden, and M. Wegener, Science **325**, 1513 (2009).
6. R. Ji, S. W. Wang, X. Liu, H. Guo, and W. Lu, ACS Photonics **3**, 2368 (2016).
7. C. Wang, Z. Li, R. Pan, W. Liu, H. Cheng, J. Li, W. Zhou, J. Tian, and S. Chen, ACS Photonics **7**, 3415 (2020).
8. X. Duan, S. Yue, and N. Liu, Nanoscale **7**, 17237 (2015).
9. Y. Cui, L. Kang, S. Lan, S. Rodrigues, and W. Cai, Nano Lett. **14**, 1021 (2014).
10. W. Zhang, B. Ai, P. Gu, Y. Guan, Z. Wang, Z. Xiao, and G. Zhang, ACS Nano **15**, 17657 (2021).
11. C. Y. Ji, S. Chen, Y. Han, X. Liu, J. Liu, J. Li, and Y. Yao, Nano Lett. **21**, 6828 (2021).
12. M. Decker, R. Zhao, C. M. Soukoulis, S. Linden, and M. Wegener, Opt. Lett. **35**, 1593 (2010).
13. Z. Li, W. Liu, H. Cheng, S. Chen, and J. Tian, Sci. Rep. **7**, 8204 (2017).
14. Z. Li, W. Liu, H. Cheng, and S. Chen, Sci. China Phys. Mech. Astron. **63**, 284202 (2020).
15. M. Zhang, Q. Lu, and H. Zheng, J. Opt. Soc. Am. B **35**, 689 (2018).
16. S. Fasold, S. Linß, T. Kawde, M. Falkner, M. Decker, T. Pertsch, and I. Staude, ACS Photonics **5**, 1773 (2018).
17. J. Mun, M. Kim, Y. Yang, T. Badloe, J. Ni, Y. Chen, C. W. Qiu, and J. Rho, Light: Sci. Appl. **9**, 139 (2020).
18. I. Fernandez-Corbaton, M. Fruhnert, and C. Rockstuhl, Phys. Rev. X **6**, 031013 (2016).
19. A. Y. Zhu, W. T. Chen, A. Zaidi, Y. W. Huang, M. Khorasaninejad, V. Sanjeev, C. W. Qiu, and F. Capasso, Light: Sci. Appl. **7**, 17158 (2018).
20. K. Tanaka, D. Arslan, S. Fasold, M. Steinert, J. Sautter, M. Falkner, T. Pertsch, M. Decker, and I. Staude, ACS Nano **14**, 15926 (2020).
21. M. V. Gorkunov, A. A. Antonov, and Y. S. Kivshar, Phys. Rev. Lett. **125**, 093903 (2020).
22. M. V. Gorkunov, A. A. Antonov, V. R. Tuz, A. S. Kupriianov, and Y. S. Kivshar, Adv. Opt. Mater. **9**, 2100797 (2021).
23. F. Zhang, M. Pu, X. Li, P. Gao, X. Ma, J. Luo, H. Yu, and X. Luo, Adv. Funct. Mater. **27**, 1704295 (2017).
24. Q. Fan, M. Liu, C. Zhang, W. Zhu, Y. Wang, P. Lin, F. Yan, L. Chen, H. J. Lezec, Y. Lu, A. Agrawal, and T. Xu, Phys. Rev. Lett. **125**, 267402 (2020).
25. S. Yu, J. Cheng, Z. Li, W. Liu, H. Cheng, J. Tian, and S. Chen, ChemPhysMater **1**, 6 (2022).
26. A. Arbabi, Y. Horie, M. Bagheri, and A. Faraon, Nat. Nanotechnol. **10**, 937 (2015).
27. D. T. Pierce and W. E. Spicer, Phys. Rev. B **5**, 3017 (1972).
28. Z. Li, W. Liu, C. Tang, H. Cheng, Z. Li, Y. Zhang, J. Li, S. Chen, and J. Tian, Adv. Theory Simul. **3**, 1900216 (2020).